Desalination and Water Treatment
www.deswater.com
doi: 10.5004/dwt.2023.29906

307 (2023) 153–161
September

Efficient adsorption of fluoride ions by polyethyleneimine modified diatomite under different conditions in a fixed bed column

Yanzhuo Zhang[a,b,*], Haiqin Zhang[a], Jing Zhao[b], Xiaozhuan Zhang[b], Zhiguo Cao[a], Binbin Jiang[a]

[a]*Water Resource Protection and Utilization in Coal Mining, Beijing 100011, China, emails: zhangadsorption@126.com (Y. Zhang), 20039431@ceic.com (H. Zhang), 10000665@ceic.com (Z. Cao), 20029907@ceic.com (B. Jiang)*
[b]*School of Environment, Henan Normal University, Key Laboratory for Yellow River and Huai River Water Environmental and Pollution Control, Ministry of Education, Henan Key Laboratory for Environmental Pollution Control, International Joint Laboratory on Key Techniques in Water Treatment, Xinxiang, Henan 453007, China, email: zjjb19980315@163.com (J. Zhao), zhangxiaozhuan0103@126.com (X. Zhang)*

Received 24 March 2023; Accepted 21 August 2023

ABSTRACT

This study investigated the removal efficiency of fluoride ions (F^-) using polyethyleneimine modified diatomite earth (PEI&DT) in a fixed bed column under different conditions. Scanning electron microscopy showed that the PEI&DT had high porosity and thermogravimetric analysis showed that the diatomite was successfully modified by polyethyleneimine (PEI). Adsorption of F^- by PEI&DT was measured in the fixed bed column using breakthrough time and saturation time, which increased with increasing bed height, but decreased with increasing F^- concentration and flow rate. The Thomas model, which had a very good fit (average = $R^2 > 0.9632$), showed that the maximum q_0 value was 97.06 mg/g. The Yoon–Nelson model predicted theoretical required times (τ_{theo}) were close to the experimental values (τ_{exp}), and the mean error (β) < 9% showed the model was accurate. These results demonstrated that PEI&DT has high potential as an adsorbent for the removal of F^- in a fixed bed column.

Keywords: Adsorption; Fluoride ions; Polyethyleneimine; Fixed bed column

1. Introduction

Coal mining by state energy groups is predominantly concentrated in northwest China [1]. As part of the coal mining process, large amounts of mine water are produced. This water represents a water resource that, if not used, will be wasted [2]. To protect and conserve water resources, national energy groups in China have built dozens of underground reservoirs to store water. However, after more than 10 y of work, while water resources have been fully protected, water quality problems in the underground reservoirs have become apparent [3]. Due to the fluoride in underground rocks, local reservoir water often has an excess of fluoride ions (F^-), with F^- concentrations exceeding 5 mg/L [4]. F^- is an important trace element in the human body, and in small amounts fluorine can protect teeth [5]. However, high levels of F^- in water can also lead to dental fluorosis in children and skeletal fluorosis in adults [6]. Therefore, an effective method for the efficient removal of F^- from water is required.

* Corresponding author.

There are multiple methods for the removal of F^- from water, among which adsorption technology is the most efficient [7]. Adsorption technologies are based on the selection of adsorbent materials with the best available F^- adsorption modes. The adsorbent diatomite, which is mainly composed of silicon dioxide, has a large specific surface area, and has stable physical and chemical properties, is suitable for the adsorption of cationic pollutants [8]. These characteristics also make diatomite very suitable for use as a carrier of modified reagents [9]. However, the surface of diatomite is negatively charged in aqueous solutions, so it cannot effectively adsorb F^-, which has a negative charge [10]. Therefore, polyethyleneimine (PEI), which is a water-soluble cationic polymer, is often used as a modification reagent [11]. After diatomite is modified with PEI, the protonated amino groups on the surface become well suited for the adsorption of anionic pollutants [12]. Usman and Khan [13] demonstrated the effectiveness of PEI using a PEI modified hollow sponge to adsorb dyes, achieving a maximum saturated adsorption capacity of 1,666.67 mg/g. Similarly, Gao et al. [14] used a PEI modified silica gel to adsorb heavy metals, achieving maximum saturated adsorption capacities ranging from 25.94 to 50.01 mg/g.

In addition to selecting a suitable absorbent, it is important to select an appropriate adsorption method. Most studies have focused on batch adsorption processes. However, batch adsorption can only reach the theoretical adsorption capacity, and the actual adsorption capacity is often much lower than that [15]. The fixed bed column method uses a column of a fixed specific height filled with adsorbent and is often used in adsorption processes. This method is more suited to actual water treatment applications because the actual adsorption occurs within a dynamic liquid flow process [16]. Furthermore, the fixed bed column method can deal with a large number of pollutants. More importantly, the fixed bed can facilitate dynamic adsorption, enabling it to treat much more water than batch adsorption [17]. Mohan et al. [18] used rGO/ZrO_2 in a fixed bed column to adsorb F^- and achieved a maximum saturated adsorption capacity of 45.7 mg/g. Ye et al. [19] used magnesia-pullulan composite as the adsorbent to adsorb F^- in a fixed bed column and achieved a maximum saturated adsorption capacity of 6.21 mg/L. The F^- adsorption process in a fixed bed is more complicated than that in the batch adsorption process, which means that the experimental parameters need to be optimized for different adsorbents [20]. However, few studies have used PEI modified diatomite to adsorb F^- in a fixed bed column, so it is necessary to further study and optimize the PEI modified diatomite F^- adsorption process to ensure the efficiency of water treatment applications.

In this work, diatomite was modified by PEI to adsorb F^- in water in a fixed bed column process. The adsorption efficiency of the adsorbent in the fixed bed was examined with different column heights, different initial concentrations of F^-, and different flow rates. The main objectives were to (1) determine the influence of different operating parameters on adsorption of F^- by modified diatomite; (2) describe the dynamic adsorption model using the optimal experimental parameters and predict the saturated adsorption capacity; (3) elucidate the mechanisms of the dynamic adsorption process.

2. Materials and methods

2.1. Modification process of diatomite

Diatomite was purchase from Aladdin Co., Ltd., (Shanghai, China). There was no further purification of the diatomite, which was white in color.

The modification process was as follows: firstly, 60 g of diatomite was mixed with 5 mL of PEI solution in 1,000 mL deionized water. The mixture was thoroughly stirred using a magnetic agitator at a rate of 600 rpm. After 6 h, stirring was stopped and the supernatant was skimmed off after 2 h of precipitation. The precipitated samples were then dried in an air blast drying oven at 80°C for 48 h. Finally, the dried modified diatomite was ground, screened through 60 mesh (0.25 mm), and sealed for preservation. The PEI modified diatomite, hereafter called PEI&DT, was light yellow in color.

2.2. Reagents

The F^- solution was prepared using NaF reagent to make a 1,000 mg/L stock solution. NaF was purchase from Sinopharm Group Co., Ltd., (China). HCl and NaOH were purchased from Tianjin Damao Co., Ltd., (Tianjin, China). Other reagents used in the experiments were of analytic quality.

2.3. Fixed bed column and operating parameter settings

Dynamic adsorption of F^- was conducted using modified diatomite in fixed bed columns. Fixed bed adsorption parameters included initial F^- concentration, solution flow rate, and adsorption height. The experimental F^- concentrations were 100, 200, and 300 mg/L. The experimental flow rates were 5.6, 7.5, and 9.7 mL/min. The heights of fixed bed adsorbent were set at 5, 10, and 15 cm. A schematic diagram of the column is shown in Fig. 1. The column reactor was made of glass (inner diameter = 3.0 cm). The column was filled with PEI&DT between quartz sand, and the thickness of the quartz sand above and below the PEI&DT was 0.3 cm. The flow rate was adjusted using a peristaltic pump.

2.4. Instrumentation

In this work, the concentration of F^- was determined using a fluoride ion meter (Shanghai Leici Instrument Co.,

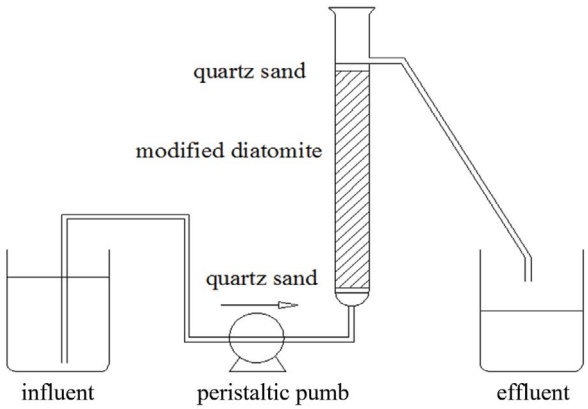

Fig. 1. Flow chart of the fixed bed process.

Ltd., China). pH was measured with a pH meter (Mettler Toledo, FE28, Switzerland). All experiments were carried out at room temperature. The surface morphology of the modified diatomite was observed by scanning electron microscopy (SEM, Hitachi S4800, Japan). The thermal stabilities of the diatomite and modified diatomite were analyzed using the thermogravimetric method (STA 409 PC, Germany). The specific surface area and pore distribution of the modified diatomite were analyzed by Brunauer–Emmett–Teller–Barrett–Joyner–Halenda (BET–BJH; Quantachrome, Autosorb iQ, USA).

2.5. Analysis of fixed bed data

The breakthrough point is when C_t reaches 10% of the C_0 [21]. The point at which effluent concentration reaches 90% is taken as the saturation point [22]. The effluent volume, V_{eff} (mL), can be calculated as follows:

$$V_{eff} = Q \times t_{totel} \tag{1}$$

The total amount of F^- adsorbed by the fixed bed is calculated using the penetration curve as follows:

$$q_{totel} = \frac{Q}{1000} \int_{t=0}^{t=t_{totel}} C_{ad} dt \tag{2}$$

where t_{total} is the total flow time; Q (mL/min) is the flow rate; and C_{ad} (mg/L) is the concentration of adsorbed F^-. q_{eq} (mg/g) is described as:

$$q_{eq} = \frac{q_{totel}}{m} \tag{3}$$

where m is the weight of the adsorbent in the fixed bed. The total amount of fluoride ion (W_{total}, mg) adsorbed by the fixed bed is calculated using Eq. (4):

$$W_{totel} = \frac{C_0 Q t_{totel}}{1000} \tag{4}$$

The removal percentage (R) of F^- can be calculated as follows:

$$R = \frac{Q_{totel}}{W_{totel}} \times 100\% \tag{5}$$

2.6. Column adsorption model

Two column adsorption models were used to analyze the experimental data, the Yoon–Nelson and Thomas models. The Thomas model is one of the most commonly models used for the adsorption properties of fixed beds. Its calculation formula is:

$$\frac{C_t}{C_0} = \frac{1}{1 + \exp\left[\frac{k_t}{Q\left(q_0 Z - C_0 V\right)}\right]} \tag{6}$$

where k_t (mL/(h·mg)) is the rate constant; V (mL) is effluent volume; q_0 is the adsorption capacity (mg/g); and Z (cm) is the height of the fixed bed.

Under different flow rates, concentrations, and column heights, there is a linear relationship between $\ln[(C_0/C_t)-1)]$ and t. The q_0 and k_t variables are calculated based on the slope and intercept of the curve. The linear relationship can be described as:

$$\ln\left(\frac{C_0}{C_t} - 1\right) = \frac{k_t q_0 m}{Q} - k_t C_0 t \tag{7}$$

The time required for the effluent F^- concentration to reach 50% C_0 was predicted, and the accuracy and error of the predicted values were determined by comparing predicted and experimental values. The Yoon–Nelson model [23] is given by Eq. (8):

$$\ln\frac{C_t}{C_0 - C_t} = k_{YN} t - \tau k_{YN} \tag{8}$$

where k_{YN} (min^{-1}) is the adsorption rate constant of the model; and τ (min) is the time required for the model to adsorb 50% of the fluorine ion concentration.

The error (β) is calculated as follows:

$$\beta = \sum_{i=1}^{N} \left| \frac{t_{exp} - t_{theo}}{t_{exp}} \right| \times 100\% \tag{9}$$

where N is the quantity of experimental data; t_{theo} is the theoretical time (min); and t_{exp} is the experimental time.

3. Results and discussion

3.1. Characteristics of the adsorbent

3.1.1. SEM analysis

As shown in Fig. S1, there were great differences in the surface microstructure of diatomite before and after modification. As can be seen in Fig. S1a, the surface of the raw diatomite was smooth and screen pores on the surface were clearly visible. This showed that the raw diatomite had a large specific surface area. After diatomite was modified (Fig. S1b), its surface was smooth and its pores were partially blocked by modification reagent, which may have reduced its specific surface area [24]. After modification, although PEI almost covered the surface of the diatomite, its micropores still existed, which meant it retained a great potential for adsorption of F^-.

3.1.2. Thermogravimetric analysis

The successful loading of PEI onto raw diatomite was confirmed by thermogravimetric analysis. The corresponding weight loss curves for raw diatomite and PEI&DT are shown in Fig. S2. For raw diatomite, free water and structural water gradually disappeared from as the temperature increased from 20°C to 250°C. For PEI&DT, there was a similar decreasing trend in weight below 250°C, but between 200°C and 650°C there was oxidative decomposition of carbohydrates in the N_2 condition [25]. When the temperature exceeded 650°C, the carbon materials gradually disappeared while SiO_2 remained. This thermal

stability test confirmed that the diatomite was successfully loaded with PEI and that the mass loss proportion of the modified diatomite was 21%.

3.1.3. BET and BJH analysis

The BET–BJH properties of raw diatomite and PEI&DT were measured, the results are listed in Table S1. The specific surface areas of PEI&DT and raw diatomite were 52.56 and 69.48 m^2/g, respectively, their average pore sizes were 10.14 and 7.21 nm, and their total pore volumes were 0.3895 and 0.4819 cm^3/g. These results showed that, although the specific surface area was reduced by PEI modification, the adsorption capacity was not negatively affected [26]. More importantly, the functional groups on the surface of PEI&DT demonstrated the ability to absorb F^- in large quantities.

3.1.4. Fourier-transform infrared spectroscopy analysis

Fig. S3 shows the Fourier-transform infrared (FTIR) spectra of the original diatomite, PEI&DT, and PEI&DT after adsorption of F^-. The characteristic peaks of the original diatomite mainly appeared at 3,442; 1,634; 1,401; 1,096; 796 and 618 cm^{-1} (Fig. S3a). The characteristic peak at 3,442 cm^{-1} was attributed to the H atom in the Si–H bond. The peak at 1,634 cm^{-1} may have been caused by the bending vibration of the H–OH bond. The characteristic peak at 1,401 cm^{-1} was attributed to the stretching vibration of the C–O bond. The characteristic peak at 1,096 cm^{-1} may have reflected the Si–O–H bond. The peaks of 796 and 618 cm^{-1} were attributed to Si–O–Si or Si–O bending vibrations.

The FTIR spectra of PEI&DT were similar to those of the original diatomite. As depicted in Fig. S3b, the new peaks after modification with diatomite, seen at wavelengths 2,389 and 2,346 cm^{-1}, were indicative of an amino group ($–NH_2$), which is the main functional group for adsorbing F^-. Fig. S3c shows that three new peaks appear after the adsorption of F^- by PEI modified diatomite. Similarly, the peaks at 1,472 and 2,354 cm^{-1} were attributed to an amino group, and the appearance of these characteristic peaks indicated that PEI had been successfully loaded on the surface of diatomite. The peak at 1,506 cm^{-1} was attributed the stretching vibration of the C=C bond.

3.1.5. Particle strength analysis

Particle strength is another effective index for evaluating adsorbents. The higher the particle's strength, the longer its life during use, and the lower the required frequency of replacement. The amount of PEI added will directly determine the adsorption capacity and the mechanical strength of adsorbent particles. Therefore, the change in particle strength was studied by adding different modifiers. As shown in Fig. S4, when the dosage of PEI reagent in the modification stage (100 g diatomite) was 10, 15, 20, and 25 mL, the particle strength of PEI&DT was 5.13, 13.26, 35.89, and 41.35 kg/cm^2. Clearly, the particle strength had a strong positive correlation with PEI volume, with a correlation coefficient (R^2) of 0.9432. According to the experimental results, when the volume of PEI was 20 mL, the particle strength efficiency peaked at 41.35 kg/cm^2.

3.2. Effects of experimental factors on F^- adsorption

3.2.1. Effect of bed height

The breakthrough point times (t_b), saturation point times (t_s), masses of adsorbed F^- (q_{eq}), and effluent volumes (V_{eff}) under different experimental conditions are shown in Table 1. Breakthrough time, saturation time, and V_{eff} of F^- were all improved with increasing bed height. As shown in Fig. 2a, the slopes of the adsorption curves gradually decreased with increasing bed height. On the one hand, the breakthrough times were 20, 85, and 186 min in the three increasing bed heights, respectively, while V_{eff} increased from 150 to 1,395 mL. On the other hand, the saturation times were 590, 780, and 1,320 min, respectively, and V_{eff} increased from 4,425 to 9,900 mL when the bed height increased from 5 to 15 cm. This phenomenon was attributed to the fact that more adsorbent was utilized for adsorption in columns with larger bed heights [27]. The increase in the height of the fixed bed increases the dosage of adsorbent. Furthermore, the increased height prolongs the residency time of F^- in the column, which increases the likelihood of contact between adsorbate and binding sites. As shown in Fig. 2a, although the concentration of F^- in the effluent reached the breakthrough point, the adsorbent was far from reaching adsorption saturation. Then, as the F^- solution continued to flow, although the concentration of F^- in the water continued to increase, the PEI&DT continued to absorb much of the F^-, resulting in the same F^- concentration in the influent and effluent [28]. Though the breakthrough point was reached quickly, adsorbent saturation took a long time. The breakthrough point and saturation point are important parameters to evaluate the adsorption performance of adsorbents. The longer the time to reach the critical value, the better the adsorption effect. In addition, electrostatic attraction is the

Table 1
Column adsorption data at C_t/C_0 = 0.1 and 0.90

C_t/C_0	Z (cm)	C_0 (mg/L)	v (mL/min)	t_b (min)	V_{eff} (mL)
0.10	5	200	7.5	20	150
0.10	10	200	7.5	85	638
0.10	15	200	7.5	186	1,395
0.10	10	100	7.5	119	893
0.10	10	200	7.5	85	638
0.10	10	300	7.5	59	443
0.10	10	200	5.6	127	711
0.10	10	200	7.5	85	638
0.10	10	200	9.7	47	458
0.90	5	200	7.5	590	4,425
0.90	10	200	7.5	780	5,850
0.90	15	200	7.5	1,320	9,900
0.90	10	100	7.5	900	6,750
0.90	10	200	7.5	780	5,850
0.90	10	300	7.5	540	4,050
0.90	10	200	5.6	1,177	6,591
0.90	10	200	7.5	780	5,850
0.90	10	200	9.7	617	5,985

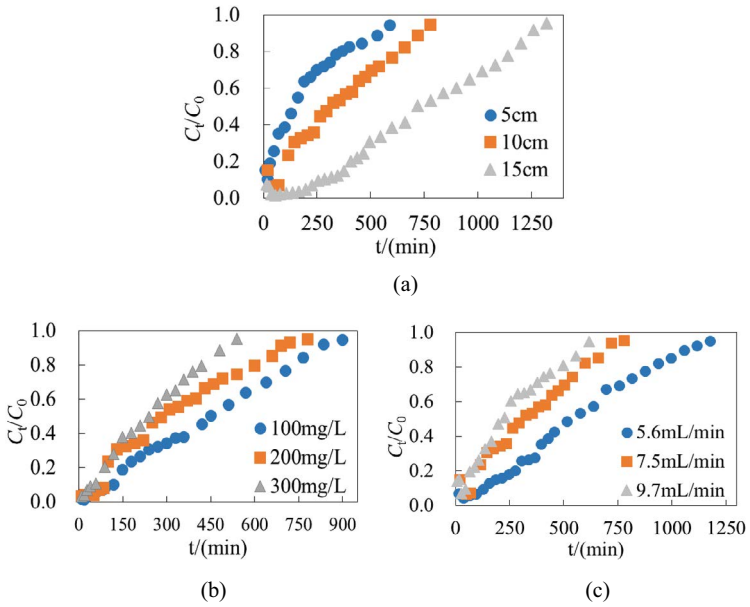

Fig. 2. Fixed bed adsorption curves for adsorption of F^- under different condition.

main mechanism of adsorption of F^- by PEI&DT. In fixed bed adsorption process, H^+ will protonate the $–NH_2$ on the surface of PEI&DT to NH_3^+ in aqueous solution [Eq. (10)].

$$\text{PEI\&DT} - NH_2 + H^+ \rightarrow \text{PEI\&DT} - NH_3^+ \quad (10)$$

$$\text{PEI\&DT} - NH_3^+ + F^- \rightarrow \text{PEI\&DT} - NH_3^+ - F^- \quad (11)$$

According to Eqs. (10) and (11), the cationic NH_3^+ in PEI&DT can attract and bind F^-. The adsorption of F^- by cationic NH_3^+ will remove it completely from solution. The principle of adsorption is generated by the mutual attraction of positive and negative charges under the action of electrostatic attraction. Under theoretical conditions, the lower the pH of the solution, the better the adsorption of F^-.

In general, the mechanism of adsorption of F^- by modified adsorbents is electrostatic attraction, and increasing the column height extends the amount of time required to reach the penetration and saturation points.

3.2.2. Effect of initial concentration

As given in Table 1, with increasing C_0, the breakthrough times t_b and saturation times t_s were 119, 85, and 59 min and 900, 780, and 540 min, which corresponded to concentrations of 100, 200, and 300 mg/L, respectively. Fig. 2b shows that, as C_0 increased, the slopes of the adsorption curves increased rapidly. This was because increases in F^- concentration in the influent led to corresponding increases in adsorbent adsorption load. In contrast, the time to reach the breakthrough point and saturation point decreased. Within the breakthrough time, V_{eff} decreased from 893 to 443 mL. Within the saturation time, V_{eff} decreased from 6,750 to 4,050 mL. As expected, lower influent concentrations resulted in longer penetration times and saturation times because lower influent concentrations were less polluting to the fixed bed. This was because the concentration gradient between PEI&DT surface and F^- in solution was increased with increasing C_0. Higher concentration differences provide a stronger driving force for the adsorption process [29]. However, the adsorption efficiency and the adsorption rate were also improved.

In general, the concentration of F^- in aqueous solution was negatively correlated with t_b and t_s. Furthermore, the adsorption of F^- by adsorbents was influenced by the strength of the gradient created by the difference between adsorption sites and F^- concentration.

3.2.3. Effect of flow rate

As the curves in Fig. 2c show, adsorption breakthrough and adsorption saturation were better at lower flow rates. As shown in Table 1, t_b, t_s, and V_{eff} decreased with increasing flow rate. The t_b values were 127, 85, and 47 min and the t_s values were 1,177, 780, and 617 min, respectively, at flow rates of 5.6, 7.5, and 9.7 mL/min. This was because, the higher the flow rate, the shorter the contact time between F^- and adsorbent. Therefore, fast flow rates may lead to incomplete adsorption processes and lower adsorption efficiencies. However, the increase in flow rate improved the breakthrough time, with the V_{eff} value decreasing from 151.2 to 97.0 mL. According to the mass transfer theory, the flow rate of the F^- solution is positively correlated with the mass transfer coefficient [30]. In other words, an increased flow rate around the PEI&DT would increase column adsorption rates. This phenomenon, in terms of the breakthrough and saturation times, can be explained as follows: when the flow rate is low, F^- gets more time to contact the adsorbent which increases the likelihood of finding the bonding points on the adsorbent. In contrast, when the flow rate is faster, the contact time between F^- and adsorbent is reduced, along with the likelihood of binding to the adsorbent's adsorption sites or within the adsorbent.

In general, changes in the flow rate affected the contact time between PEI&DT and F^-. The flow rate was negatively correlated with t_s and t_b.

3.3. Application of the Thomas model

The experimental data were analyzed using the Thomas model and the penetration curves of F^- on PEI&DT at different flow rates, concentrations, and column heights were studied (Fig. 3). Table 2 shows that maximum saturated adsorption capacity (q_0) increased with increasing bed height but decreased with increasing flow rate and F^- concentration. The result was that the more adsorbent there is, the larger its adsorption capacity. The Thomas model confirmed that the q_0 was achieved at a flow of 7.5 mL/min, a concentration of 100 mg/L, and a bed height of 5 cm. However, k_t remained high when there were high F^- concentrations, high flow rates, and large bed heights. This phenomenon showed that q_0 was increased at lower concentrations, flow rates, and bed heights, while k_t was decreased at higher concentrations, flow rates, and bed heights. The average R^2 value of the Thomas model was 0.9700, showing that this model had an excellent fit and indicating that the model is suitable for describing column data. Table 3 shows a comparison of the adsorption capacities of different materials when adsorbing F^- under different experimental conditions using the Thomas model. Based on the comparison, PEI&DT is the best adsorbent for the adsorption of F^- [31–36].

3.4. Application of Yoon–Nelson model

The experimental data were fitted into the Yoon–Nelson model to determine the breakthrough curve of F^- on PEI&DT (Fig. 4). The k_{YN} and τ_{theo} values were obtained under different experimental conditions by fitting the adsorption curves. Table 4 shows that k_{YN} increased as the F^- concentration increased. The theoretical times (τ_{theo}) for the concentration of F^- in solution to reach 50% of the inlet water concentration were close to the experimental times (τ_{exp}). Their errors (β) were all below 9% and their $R^2 > 0.96$. The fitting results showed that the adsorption process of the modified adsorbent was normal, and the model can be used to fit effectively. Therefore, the Yoon–Nelson model can accurately describe the dynamic adsorption process of F^- on PEI&DT. These agreed with Vieira et al. [37], who concluded that these two dynamic adsorption models are suitable for describing experimental breakthrough curves.

Table 2
Thomas model parameters with different factors of column adsorption

Z (cm)	C_0 (mg/L)	v (mL/min)	q_0 (mg/g)	k_1 (mL/min)	R^2
10	100	7.5	29.20	0.069	0.9613
10	200	7.5	20.89	0.065	0.9799
10	300	7.5	15.95	0.101	0.9706
10	100	5.6	36.46	0.048	0.9855
10	100	7.5	20.37	0.058	0.9814
10	100	9.7	15.96	0.076	0.9660
5	100	7.5	97.06	0.046	0.9501
10	100	7.5	20.89	0.054	0.9800
15	100	7.5	7.25	0.070	0.9548

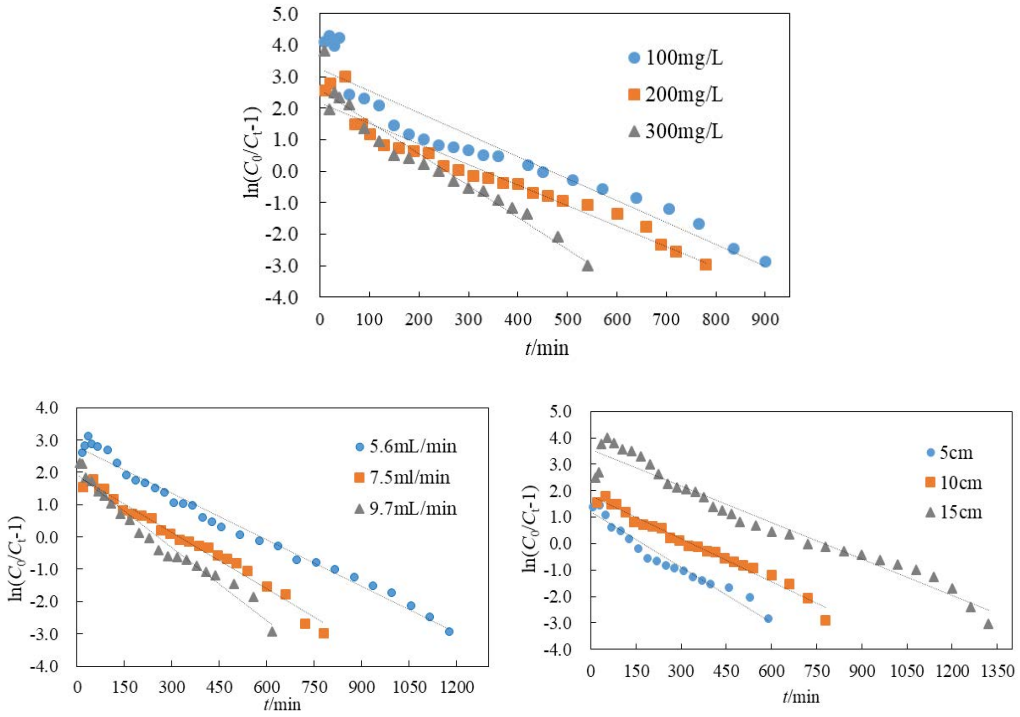

Fig. 3. Adsorption curves of F^- on PEI&DT according to the Thomas model.

Table 3
Comparison of F^- adsorption capacity of PEI&DT with the reported adsorbents

Adsorbents	Adsorption capacity q_0 (mg/L)	References
Red mud-based geopolymer microspheres	76.57	[31]
Amorphous porous Al_2O_3 microfiber clusters	10.82	[32]
Chitosan-praseodymium	15.87	[33]
Manganese carbonate ($MnCO_3$) nanowire	46.80	[34]
NH_2-UiO-66	65.08	[35]
Nanostructured porous MgO hollow spheres	175.00	[36]
PEI&DT	97.06	This study

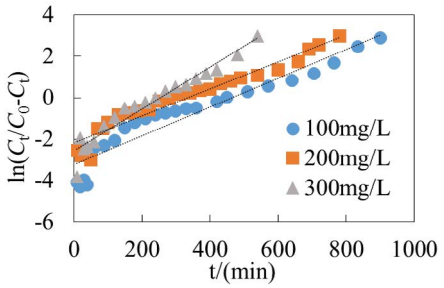

Fig. 4. Adsorption curves of F^- on PEI&DT according to the Yoon–Nelson model.

Table 4
Yoon–Nelson model parameters for DE@C

Z (min)	v (mL/min)	C_0 (mg/L)	k_{YN} (min)	τ (min)	τ (exp)	R^2
10	7.5	100	0.0054	420.7	450.0	0.9613
10	7.5	200	0.0057	305.1	280.0	0.9799
10	7.5	300	0.0091	266.5	239.0	0.9706

4. Conclusion

In this work, the use of PEI modified diatomite as a potential adsorbent for F^- in a fixed bed system was tested under different experimental conditions. SEM confirmed that the modified diatomite surface was covered by the modification reagent, indicating that PEI successfully coated the adsorbent surface. Thermogravimetric analysis showed that the diatomite was successfully modified by PEI. After modification, BET analysis showed that PEI&DT still had a high specific surface area. The column adsorption data showed that the breakthrough time and saturation time both increased with increasing bed height but decreased with increasing flow rate and F^- concentration. The Thomas model showed that the q_0 of dynamic adsorption was 97.06 mg/g. The theoretical values predicted by the Yoon–Nelson model were very close to the actual values, with an average β < 9%. This study demonstrated that this material could serve as an effective adsorbent for F^- removal from aqueous solution in a fixed bed column adsorption system.

Acknowledgement

This work was supported by the Open Fund of the State Key Laboratory of Water Resource Protection and Utilization in Coal Mining (Grant No. GJNY-18-73.14), the National Natural Science Foundation of China (Grants No. 52000060), and the Henan provincial key science and technology research project (222102110136).

References

[1] I. Tarasenko, A. Kholodov, A. Zin'kov, I. Chekryzhov, Chemical composition of groundwater in abandoned coal mines: evidence of hydrogeochemical evolution, Appl. Geochem., 137 (2022) 105210, doi: 10.1016/j.apgeochem.2022.105210.
[2] Z. Yang, W. Li, X. Li, J. He, Quantitative analysis of the relationship between vegetation and groundwater buried depth: a case study of a coal mine district in Western China, Ecol. Indic., 102 (2019) 770–782.
[3] Z. Yan, G. Liu, R. Sun, Q. Tang, D. Wu, B. Wu, C. Zhou, Geochemistry of rare earth elements in groundwater from the Taiyuan Formation limestone aquifer in the Wolonghu Coal Mine, Anhui province, China, J. Geochem. Explor., 135 (2013) 54–62.
[4] T. Rinder, M. Dietzel, J.A. Stammeier, A. Leis, D. Bedoya-González, S. Hilberg, Geochemistry of coal mine drainage, groundwater, and brines from the Ibbenbüren mine, Germany: a coupled elemental-isotopic approach, Appl. Geochem., 121 (2020) 104693, doi: 10.1016/j.apgeochem.2020.104693.
[5] M. Gomo, D. Vermeulen, Hydrogeochemical characteristics of a flooded underground coal mine groundwater system, J. Afr. Earth Sci., *92* (2014) 68–75.
[6] L. Li, W. Li, Q. Wang, Prediction and zoning of the impact of underground coal mining on groundwater resources, Process Saf. Environ. Prot., *168* (2022) 454–462.
[7] C. Jiang, L. Cheng, C. Li, L. Zheng, A hydrochemical and multi-isotopic study of groundwater sulfate origin and contribution in the coal mining area, Ecotoxicol. Environ. Saf., 248 (2022) 114286, doi: 10.1016/j.ecoenv.2022.114286.
[8] M. Zhu, B. Li, G. Liu, Groundwater risk assessment of abandoned mines based on pressure-state-response—the example of an abandoned mine in southwest China, Energy Rep., 8 (2022) 10728–10740.
[9] D. Guo, H. Li, J. Wang, Z. Xu, Facile synthesis of NH_2-UiO-66 modified low-cost loofah sponge for the adsorption of fluoride from water, J. Alloys Compd., 929 (2022) 167270, doi: 10.1016/j.jallcom.2022.167270.
[10] K. Li, Z. Hu, R. Zhao, J. Zhou, C. Jing, Q. Sun, J. Rao, K. Yao, B. Dong, X. Liu, H. Li, Y. Zang, J. Ji, A multidimensional rational design of nickel–iron sulfide and carbon nanotubes on diatomite via synergistic modulation strategy for supercapacitors, J. Colloid Interface Sci., 603 (2021) 799–809.
[11] X. Chen, J. Lin, H. Wang, Y. Yang, C. Wang, Q. Sun, X. Shen, Y. Li, Epoxy-functionalized polyethyleneimine modified

epichlorohydrin-cross-linked cellulose aerogel as adsorbents for carbon dioxide capture, Carbohydr. Polym., 302 (2023) 120389, doi: 10.1016/j.carbpol.2022.120389.
[12] B. Gao, P. Jiang, F. An, S. Zhao, Z. Ge, Studies on the surface modification of diatomite with polyethyleneimine and trapping effect of the modified diatomite for phenol, Appl. Surf. Sci., 250 (2005) 273–279.
[13] M.A. Usman, A.Y. Khan, Selective adsorption of anionic dye from wastewater using polyethyleneimine based macroporous sponge: batch and continuous studies, J. Hazard. Mater., 428 (2022) 128238, doi: 10.1016/j.jhazmat.2022.128238.
[14] B. Gao, F. An, K. Liu, Studies on chelating adsorption properties of novel composite material polyethyleneimine/silica gel for heavy-metal ions, Appl. Surf. Sci., 253 (2006) 1946–1952.
[15] T.B. da Costa, T.L. da Silva, C.S. Dias Costa, M.G.C. da Silva, M.G.A. Vieira, Chromium adsorption using *Sargassum filipendula* algae waste from alginate extraction: batch and fixed-bed column studies, Chem. Eng. J. Adv., 11 (2022) 100341, doi: 10.1016/j.ceja.2022.100341.
[16] J.S. da Costa, A.R. Fajardo, Polypyrrole/stearic acid-coated *Luffa cylindrica* for enhanced removal of sodium diclofenac from water: batch and continuous adsorption studies, J. Cleaner Prod., 389 (2023) 136084, doi: 10.1016/j.jclepro.2023.136084.
[17] L. Hu, Y. Wu, M. Li, X. Zhang, X. Xian, Y. Mai, X. Lin, Highly selective adsorption of 5-hydroxymethylfurfural from multicomponent mixture by simple pH controlled in batch and fixed-bed column studies: competitive isotherms, kinetic and breakthrough curves simulation, Sep. Purif. Technol., 299 (2022) 121756, doi: 10.1016/j.seppur.2022.121756.
[18] S. Mohan, D.K. Singh, V. Kumar, S.H. Hasan, Effective removal of fluoride ions by rGO/ZrO_2 nanocomposite from aqueous solution: fixed bed column adsorption modelling and its adsorption mechanism, J. Fluorine Chem., 194 (2017) 40–50.
[19] Y. Ye, Y. Wei, Y. Gu, D. Kang, W. Jiang, J. Kang, Simultaneous removal of fluoride and phosphate in a continuous fixed-bed column filled with magnesia-pullulan composite, J. Alloys Compd., 838 (2020) 155528, doi: 10.1016/j.jallcom.2020.155528.
[20] Y. Cardona, S.A. Korili, A. Gil, Use of response surface methodology to optimize triclosan adsorption on alumina pillared clays in a fixed-bed column for applications in solid-phase extraction, Appl. Clay Sci., 235 (2023) 106879, doi: 10.1016/j.clay.2023.106879.
[21] M.B. de Farias, M.P. Spaolonzi, M.G.C. Silva, M.G.A. Vieira, Fixed-bed adsorption of bisphenol A onto organoclay: characterisation, mathematical modelling and theoretical calculation of DFT-based chemical descriptors, J. Environ. Chem. Eng., 9 (2021) 106103, doi: 10.1016/j.jece.2021.106103.
[22] K.H. Chu, Breakthrough curve analysis by simplistic models of fixed bed adsorption: in defense of the century-old Bohart–Adams model, Chem. Eng. J., 380 (2020) 122513, doi: 10.1016/j.cej.2019.122513.
[23] Y.H. Yoon, J.H. Nelson, Application of gas adsorption kinetics. I. A theoretical model for respirator cartridge service life, Am. Ind. Hyg. Assoc. J., 45 (1984) 509–516.
[24] A. Gizaw, F. Zewge, Y. Chebude, A. Mekonnen, M. Tesfaye, Simultaneous nitrate and phosphate abatement using calcium silicate hydrate adsorbent: fixed bed column adsorption study, Surf. Interfaces, 30 (2022) 101961, doi: 10.1016/j.surfin.2022.101961.
[25] Y. Fang, M. Wu, Q. Zhang, F. Zhou, C. Deng, Y. Yan, H. Shen, Y. Tang, Y. Wang, Hierarchical covalent organic frameworks-modified diatomite for efficient separation of bisphenol A from water in a convenient column mode, Sep. Purif. Technol., 298 (2022) 121611, doi: 10.1016/j.seppur.2022.121611.
[26] J. Wang, G. Zhang, S. Qiao, J. Zhou, Comparative assessment of formation pathways and adsorption behavior reveals the role of NaOH of MgO-modified diatomite on phosphate recovery, Sci. Total Environ., 876 (2023) 162785, doi: 10.1016/j.scitotenv.2023.162785.
[27] D. Ulloa-Ovares, C.E. Rodriguez-Rodriguez, M. Masís-Mora, J.E. Duran, Simultaneous degradation of pharmaceuticals in fixed and fluidized bed reactors using iron-modified diatomite as heterogeneous Fenton catalyst, Process Saf. Environ. Prot., 152 (2021) 97–107.
[28] Y. Wu, X. Li, Q. Yang, D. Wang, Q. Xu, F. Yao, F. Chen, Z. Tao, X. Huang, Hydrated lanthanum oxide-modified diatomite as highly efficient adsorbent for low-concentration phosphate removal from secondary effluents, J. Environ. Manage., 231 (2019) 370–379.
[29] R.P. Chicinaş, E. Gál, H. Bedelean, M. Darabantu, A. Măicăneanu, Novel metal modified diatomite, zeolite and carbon xerogel catalysts for mild conditions wet air oxidation of phenol: characterization, efficiency and reaction pathway, Sep. Purif. Technol., 197 (2018) 36–46.
[30] X. Liu, C. Yang, Y. Wang, Y. Guo, Y. Guo, G. Lu, Effect of the diatomite pretreatment on the catalytic performance of TS-1/diatomite for toluene hydroxylation by H_2O_2 in fixed-bed reactor, Chem. Eng. J., 243 (2014) 192–196.
[31] M. Yi, K. Wang, H. Wei, D. Wei, X. Wei, B. Wei, L. Shao, T. Fujita, X. Cui, Efficient preparation of red mud-based geopolymer microspheres (RM@GMs) and adsorption of fluoride ions in wastewater, J. Hazard. Mater., 442 (2023) 130027, doi: 10.1016/j.jhazmat.2022.130027.
[32] K. Yang, Y. Li, Z. Tian, K. Peng, Y. Lai, Removal of fluoride ions from $ZnSO_4$ electrolyte by amorphous porous Al_2O_3 microfiber clusters: adsorption performance and mechanism, Hydrometallurgy, 197 (2020) 105455, doi: 10.1016/j.hydromet.2020.105455.
[33] E. Kusrini, N. Sofyan, N. Suwartha, G. Yesya, C.R. Priadi, Chitosan-praseodymium complex for adsorption of fluoride ions from water, J. Rare Earths, 33 (2015) 1104–1113.
[34] Y.X. Zhang, Y. Jia, Fluoride adsorption on manganese carbonate: ion-exchange based on the surface carbonate-like groups and hydroxyl groups, J. Colloid Interface Sci., 510 (2018) 407–417.
[35] D. Guo, H. Li, J. Wang, Z. Xu, Facile synthesis of NH_2-UiO-66 modified low-cost loofah sponge for the adsorption of fluoride from water, J. Alloys Compd., 929 (2022) 167270, doi: 10.1016/j.jallcom.2022.167270.
[36] R. Zhu, X. Wang, J.G. Panther, Q. Wang, S. Chakir, Y. Ding, Y. Huang, H. Wang, Micro/nanostructured MgO hollow spheres with selective adsorption performance and their application for fluoride monitoring in water, Sep. Purif. Technol., 299 (2022) 121703, doi: 10.1016/j.seppur.2022.121703.
[37] M.L.G. Vieira, V.M. Esquerdo, L.R. Nobre, G.L. Dotto, L.A.A. Pinto, Glass beads coated with chitosan for the food azo dyes adsorption in a fixed bed column, J. Ind. Eng. Chem., 20 (2014) 3387–3393.

Supporting information

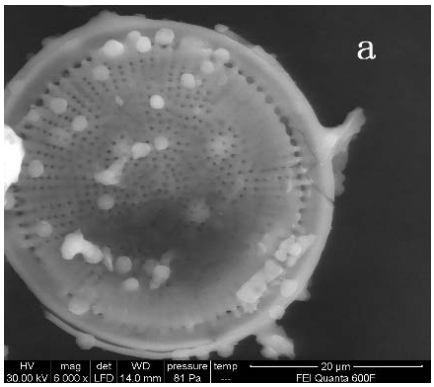

(a)

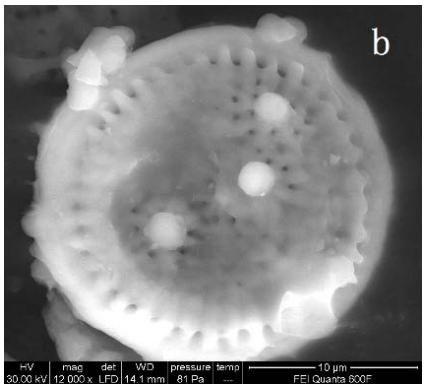

(b)

Fig. S1. Scanning electron microscopy image of (a) raw diatomite and (b) PEI&DT.

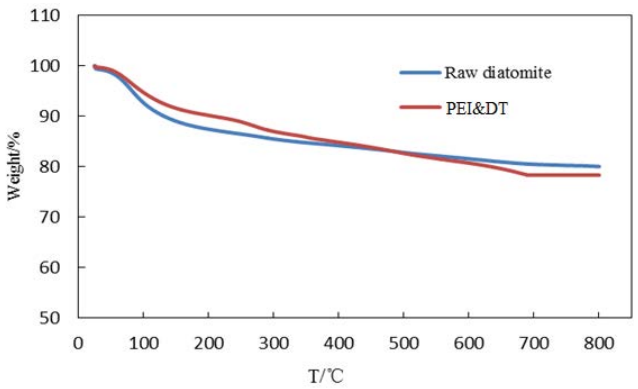

Fig. S2. Thermogravimetric analysis curves obtained in air for raw diatomite and PEI&DT.

Table S1
BET and BJH analysis of raw diatomite and PEI&DT

Name	BET (m^2/g)	Average pore (nm)	Total pore volume (cm^3/g)
Raw diatomite	69.48	7.21	0.4819
PEI&DT	52.56	10.14	0.3895

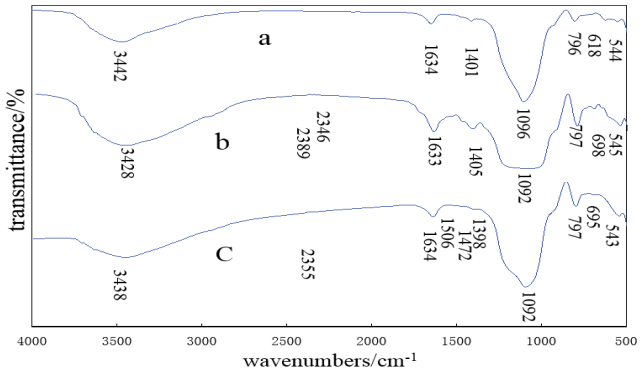

Fig. S3. Fourier-transform infrared spectra of original diatomite (a), PEI&DT (b) and PEI&DT after F^- adsorption (c).

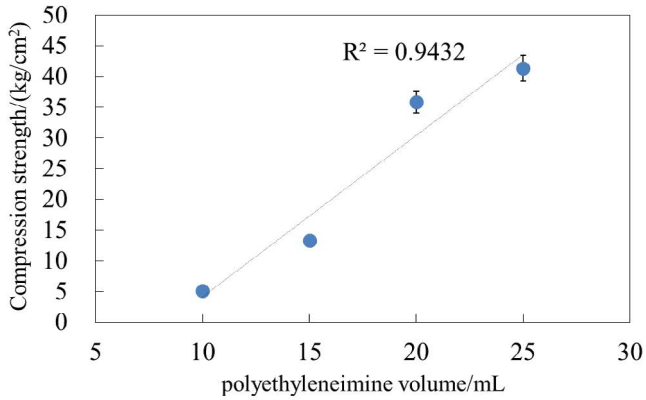

Fig. S4. Linear relationship of particle strength and PEI reagent.